14th International Symposium on Turbulence and Shear Flow Phenomena (TSFP14)
Heidelberg, Germany, July 28–31, 2026

AN EMBEDDED LES METHOD FOR TURBULENT FLOWS

Jannik Borgelt
Institute of Aerodynamics (AIA)
RWTH Aachen University
Wüllnerstraße 5a, 52062 Aachen, Germany
j.borgelt@aia.rwth-aachen.de

Matthias Meinke
Institute of Aerodynamics (AIA)
RWTH Aachen University
Wüllnerstraße 5a, 52062 Aachen, Germany
m.meinke@aia.rwth-aachen.de

Dominik Krug
Institute of Aerodynamics (AIA)
RWTH Aachen University
Wüllnerstraße 5a, 52062 Aachen, Germany
d.krug@aia.rwth-aachen.de

Wolfgang Schröder
Institute of Aerodynamics (AIA)
RWTH Aachen University
Wüllnerstraße 5a, 52062 Aachen, Germany
office@aia.rwth-aachen.de

ABSTRACT

An embedded LES (ELES) method is introduced which employs a priori defined RANS and LES regions, where a preliminary RANS solution provides physically consistent boundary conditions for a reduced LES domain. The information is exchanged between the steady RANS computation and the embedded, time-resolved LES region, which is limited in the streamwise and normal directions such that the overall computational cost and convergence time is reduced. At the inflow boundary of the ELES region, a synthetic turbulence generation method is used, which allows the introduction of freestream turbulence, which is necessary e.g. for turbomachinery flows. At the domain boundary, which is almost tangential to the main flow direction, the mass flux determined by the preliminary RANS is defined. A Navier-Stokes characteristic boundary condition capable of handling highly turbulent flows with local flow reversal is used at the outflow of the embedded LES domain. The formulation of the boundary conditions are validated for the flow over a curved backward-facing step and subsequently used to predict of the hot gas ingress into the stator-rotor cavity gap of an axial turbine geometry.

INTRODUCTION

Current computing capabilities still limit the use of scale-resolved simulations, e.g., large-eddy simulations (LES), for industrial design processes. In particular, the numerical analysis of turbomachinery flows such as sealing systems and rotor–stator cavity flows is predominantly based on the solution of the Reynolds-averaged Navier-Stokes (RANS) equations, which reliably capture key features of turbulent flows under steady or mildly unsteady conditions. Therefore, they remain widely used in the industrial design process for turbomachinery due to their low computational cost and robustness. However, their accuracy strongly depends on the turbulence model, particularly for flows with separation, curvature, or strong pressure gradients.

The prediction of the sealing effectiveness and hot gas distribution within the seal gap of stator-rotor wheel spaces in axial turbines remain challenging for RANS models due to the complex fluid dynamics within the rim seal region involving multi-mode ingress mechanisms and strong turbulent shear layers. In some cases, significant discrepancies compared to experimental measurements have been reported, see Rabs *et al.* (2009) and O'Mahoney *et al.* (2011). Previous studies have shown that high-fidelity simulations, such as large-eddy simulation (LES), can provide significantly improved predictions for hot gas ingress into the stator-rotor wheel space of axial turbines, see Gao *et al.* (2018) and Pogorelov *et al.* (2019). However, the computational cost associated with resolving the inertial range of the turbulence spectrum via LES remains prohibitively high. This motivates the development of more computationally efficient modeling strategies capable of capturing the essential unsteady flow features relevant to hot gas ingestion in rim seal geometries.

In this paper an embedded LES method is presented, in which a preliminary RANS solution is used to describe physically meaningful boundary conditions for an LES region reduced to a region of interest, with the aim of supporting the industrial design process for turbomachinery applications. Recent advances in GPU-driven simulations suggest that large-scale LES may become economically feasible for the industrial design process in the near future. The method presented in this paper aims to bridge the gap between current computational capabilities and the routine use of LES in the industrial design process.

In the following, the method is first validated for a generic curved-backward facing step geometry designed to replicate the characteristic flow conditions expected at the embedded LES interfaces in axial turbomachinery applications, with the LES domain restricted to the separation region. The developed boundary conditions for the embedded LES are adapted and subsequently used for axial turbomachinery flows and validated for the prediction of hot gas ingress into stator–rotor wheel space in a curved axial turbine cascade. Here, the embedded LES method was used to reduce the LES region to the rim seal gap.

EMBEDDED LES METHOD

A novel Navier-Stokes characteristic boundary condition (NSCBC) is used at the outflow of the embedded LES domain, as presented in Borgelt *et al.* (2025*a*). The boundary formulation is capable of handling highly turbulent flows with local flow reversal by detecting these local flow reversal events and switching the boundary formulation accordingly. The amplitude of the characteristic wave for outflow events utilizes the pressure field, and for local inflow events the velocity and temperature field of a preliminary RANS encompassing the full domain. In the simulation, the Spalart-Allmaras turbulence model was used. The adopted boundary formulation enables the embedded LES interface to be placed in highly turbulent regions thereby reducing its overall extent. The wall-parallel or tangential zonal interface (TZI) further reduces the extent of the embedded LES region to the near wall and separation region. In general, this boundary condition is nearly aligned with the velocity field at the inflow of the embedded LES. However, in general a mean mass flux can exist on this boundary, which has to be taken into account. The present boundary formulation allows the correct mass flux determined by the preliminary RANS to enter or exit the embedded LES domain over the boundary surface without prescribing inflow turbulence or sampling it from inside the embedded LES domain, see Borgelt *et al.* (2025*a*). This method gave good results if the tangential interface is placed outside the turbulent boundary layer. These boundary conditions are combined with the reformulated synthetic turbulence generation (RSTG) method by Roidl *et al.* (2013) at the inflow, which is used to generate turbulent velocity fluctuations from the time-averaged values of the preliminary RANS solution. To efficiently simulate axial turbine flow the RSTG method is extended to include the generation of freestream turbulence as presented in Borgelt *et al.* (2025*b*). This extension is particularly important due to its influence on boundary layer separation on the stator blade, which in turn significantly affects the pressure distribution on the blade surfaces and the resulting hot gas ingress as well as the shear-layer dynamics. The simulation of axial turbine geometries that include the curvature require additional adaptations to the RSTG method which are discussed in the following.

Curvature adaptations to the RSTG method

The synthetic turbulence generation method is adapted for turbine geometries that include curvature by creating the velocity fluctuations in the $(x, r\theta, r)$-coordinate system. A schematic of an inflow of a curved axial turbine cascade and the coordinate transformation is depicted in figure 1. The velocity fluctuations $\hat{u}'_m$ induced by the virtual eddies at a point $(x, r\theta, r, t)$ in the inlet plane of the embedded LES are computed by

$$\hat{u}'_m(x, r, r\theta, t) = \sum_{n=1}^{N} \underbrace{\Theta_m^n f_{l_x,m}(\tilde{x}) f_{l_r,m}(\tilde{r}) f_{l_{r\theta},m}(\tilde{r\theta})}_{u_m^n(x, r\theta, r, t)}. \qquad (1)$$

The influence of a particular eddy core on a point in the LES inlet plane is calculated using the shape functions $f_{l_x,m}$, $f_{l_r,m}$, $f_{l_{r\theta},m}$ as defined in Roidl *et al.* (2013). The transformation to the $(x, r\theta, r)$ coordinate system ensures correct eddy scales in the radial direction. The instantaneous velocity fluctuations are scaled by the Cholesky decomposition, in the $(x, r\theta, r, t)$-coordinate system given by

$$u'_m(x, r\theta, r, t) = \sum_n A_{mn} \hat{u}'_m(x, r\theta, r, t). \qquad (2)$$

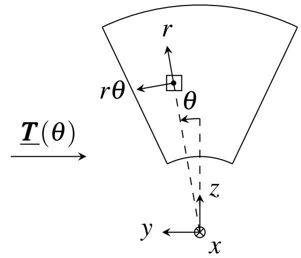

Figure 1. Schematic of the coordinate transformation from Cartesian (x, y, z)- to the $(x, r\theta, r)$ coordinates at the RSTG inflow plane for a curved turbine cascade setup.

The instantaneous velocity components at the LES inlet plane at the Cartesian point (x, y, z, t) are obtained by superimposing the time-averaged RANS velocity field with the scaled velocity fluctuations. They are transformed to the Cartesian coordinate system, i.e.,

$$u_{\mathrm{LES},m} = u_{\mathrm{RANS},m} + \sum_{d=1}^{3} T_{md} u'_d(x, r\theta, r, t). \qquad (3)$$

The quantity T_{md} denotes the entries of the inverse of the rotation tensor $\underline{\boldsymbol{T}}$ given as

$$\underline{\boldsymbol{T}}(\theta) = \begin{pmatrix} 1 & 0 & 0 \\ 0 & \cos(\theta) & -\sin(\theta) \\ 0 & \sin(\theta) & \cos(\theta) \end{pmatrix}. \qquad (4)$$

The Reynolds stress tensor components needed for the similarity relation used in the Cholesky decomposition is transformed in the $(x, r\theta, r)$-coordinate system by the tensor rotation

$$\underline{\tau}'_t = \begin{pmatrix} \overline{u'u'} & \overline{u'v'_\theta} & \overline{u'v'_r} \\ \overline{u'v'_\theta} & \overline{v'_\theta v'_\theta} & \overline{v'_\theta v'_r} \\ \overline{u'v'_r} & \overline{v'_\theta v'_r} & \overline{v'_r v'_r} \end{pmatrix} = \underline{T}\,\underline{\tau}_t \underline{T}_t^{\mathsf{T}}. \qquad (5)$$

Here, v_r is the radial velocity component and v_θ is the tangential velocity component in cylindrical coordinates. The azimuthal angle in cylindrical coordinates θ is defined by its Cartesian coordinates $\theta = \arctan\left(\frac{y}{z}\right)$.

CURVED BACKWARD-FACING STEP

In the following, the embedded LES method is validated for the flow over a curved backward-facing step. The performance of the method is assessed through comparisons with the preliminary RANS solution and a reference full-domain LES simulation.

Geometry and numerical setup

The efficiency and the accuracy of the method is first demonstrated on separating flow over a curved backward-facing step, in which the embedded LES region is limited to the separation region, as shown in figure 2. The geometry of the curved backward-facing step is equal to the backward step of the periodic hill geometry, which is defined on NASA's website on turbulence models Langley Research Center (2021). The Reynolds number, based on the bulk velocity

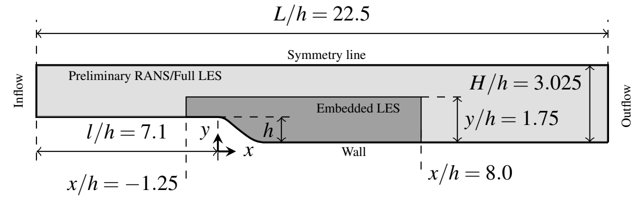

Figure 2. Geometry of the curved backward-facing step, the total domain, the embedded domains, and the boundary conditions.

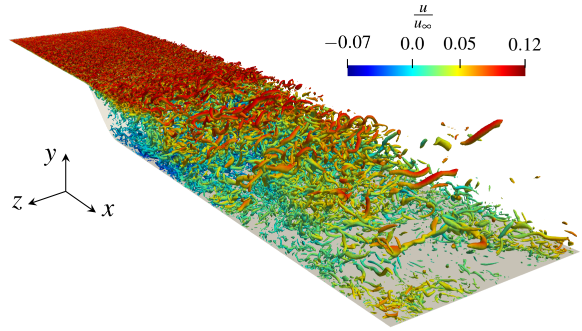

Figure 3. Q-criterion contours colored by the instantaneous streamwise velocity component u of pure LES reference solution.

at the crest of the step and the step height h, is $Re_h = 28{,}000$ at a Mach number of $M = 0.1$. The computational domain extends $7.1h$ upstream of the curved backward-facing step. The non-dimensional domain height and total length are given by $H/h = 3.025$ and $L/h = 22.5$, respectively, while the spanwise width is $4.5h$ with periodic boundary conditions applied in that direction. The inflow location of the embedded LES region is positioned at $x/h = -1.25$, corresponding to a distance of approximately 7δ upstream of the step onset at $x/h = 0.0$, with δ being the boundary-layer thickness at that location. The wall-normal position of the tangential zonal interface is set to $y/h = 1.75$. A no-slip boundary condition is imposed at the wall, which is assumed to be adiabatic.

In the full LES setup, turbulence is introduced at the inflow with a prescribed turbulent intensity of 5%, using the turbulence generation method proposed by Batten *et al.* (2004). The outflow boundary is modeled using the NSCBC formulation of Granet *et al.* (2010), where the target pressure is set as the free-stream pressure, p_∞. In contrast, the full RANS setup applies a standard outflow boundary condition with the pressure fixed to p_∞. For both the full LES and full RANS setups, the upper boundary is treated using a symmetry condition.

The grid of the full LES setup consists of 151 million cells. The zonal setup has a grid size of 91 million cells, corresponding to a reduction in grid cells of 40%. The 2D-RANS setup has a grid size of approximately two million cells. The data is summarized in table 1.

Table 1. Number of grid cells employed for the different setups for the curved backward-facing step geometry.

	RANS	LES	embedded LES
grid cells [10^6]	2	151	91

Simulation results

The performance of the embedded LES method is assessed through comparisons with the preliminary RANS solution and a reference full-domain LES simulation. To provide an impression of the flow structures, figure 3 shows Q-criterion contours colored by the instantaneous streamwise velocity component u obtained from the full-domain LES reference solution.

Figure 4 shows the wall-normal distributions of the streamwise velocity component u at several streamwise locations for the different simulation methods. The full RANS solution agrees well with the velocity profiles from the full-domain LES outside the recirculation region. The recirculation region is visualized by the contour line $u/u_\infty = 0$. The size of the recirculation region predicted by RANS is underestimated. In contrast, the embedded LES setup shows a very good agreement in the streamwise velocity component u and the extent of the recirculation region compared to the full LES setup.

The wall-shear stress distribution τ_w is presented in figure 4 (bottom). The reattachment position is identified by the point at which the wall-shear stress vanishes at the wall $y/h = 0$. The full RANS setup exhibits a misprediction of the wall-shear stress along the entire lower wall. Specifically, the reattachment location predicted by the full RANS solution occurs at $x/h = 7.43$, which deviates significantly from the full LES prediction of $x/h = 6.6$. In contrast, the embedded LES approach accurately reproduces the reattachment location, showing excellent agreement with the full LES result. Furthermore, the NSCBC outflow formulation does not introduce any detectable upstream influence on the velocity field. This conclusion is supported by the consistency of the wall-shear stress distribution in the vicinity of the embedded LES outflow boundary at $x/h = 8.0$.

The wall-normal distributions of the Reynolds shear stress

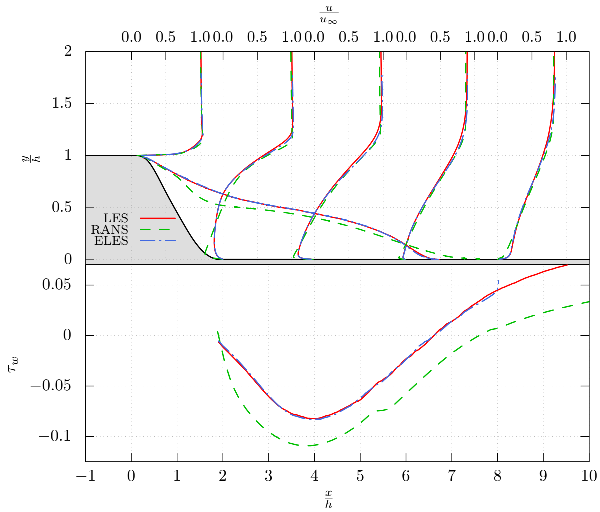

Figure 4. (top) Wall-normal velocity distribution of the time-averaged streamwise velocity component u/u_∞, (bottom) non-dimensionalized wall-shear stress τ_W on the leeward wall of the curved backward-facing step at $y/h = 0.0$; LES: full LES, RANS: full RANS, ELES: embedded LES.

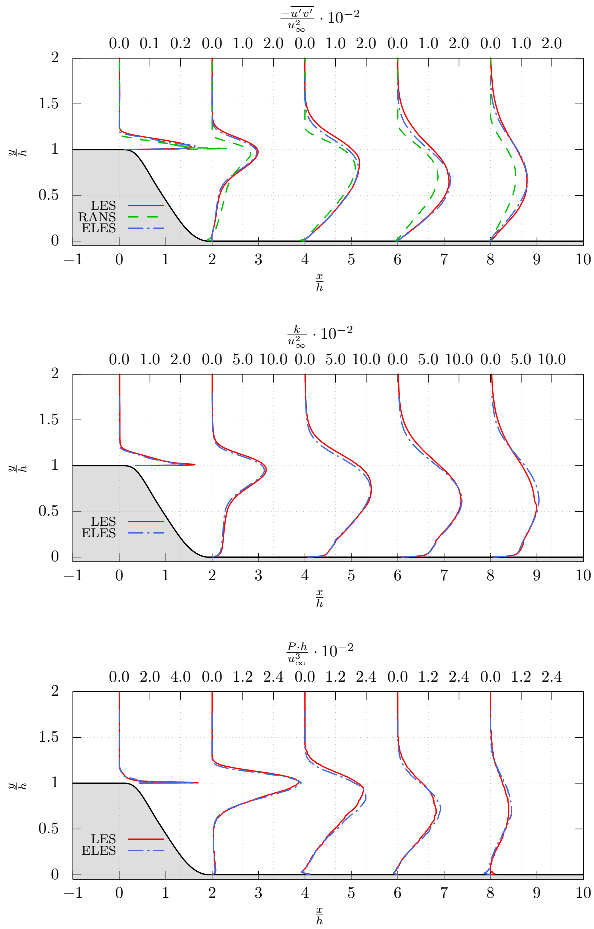

Figure 5. Wall-normal distributions of (top) the Reynolds shear stress $\overline{u'v'}$, (middle) the turbulent kinetic energy k, and (bottom) the production of turbulent kinetic energy P non-dimensionalized by u_∞; LES: full LES, RANS: full RANS, ELES: embedded LES.

and $\overline{u'v'}$, and the turbulent kinetic energy k, the production of the turbulent kinetic energy P are shown in figure 5. A very good agreement between the embedded LES and the full LES solution is observed. The embedded LES shows a massive improvement compared to the RANS solution especially inside the recirculation region. At the outflow, i.e., $x/h = 8.0$, the production term of turbulent kinetic energy is positive near the wall in the full LES data, whereas the embedded LES predicts negative values. This discrepancy can be attributed to the NSCBC outflow formulation, which enforces negative instantaneous velocities toward the positive time-averaged RANS state. As a consequence, a negative turbulent kinetic energy production term arises, predominantly in the near-wall region.

AXIAL TURBINE SETUP

The adaptation to the embedded LES method for turbomachinery application is validated for a curved stator cascade consisting of the first stator row and wheel space of the ICAS-GT2 turbine geometry investigated. The turbine geometry was originally studied experimentally as well numerically by Jakoby *et al.* (2004). Later, Hösgen *et al.* (2023, 2024) improved the numerical predictions of Jakoby *et al.* (2004) by conducting detailed high-fidelity LES simulations of the same geometry and operating conditions. The focus of the analysis is on the accurate prediction of the hot gas ingress into the stator-rotor wheel space.

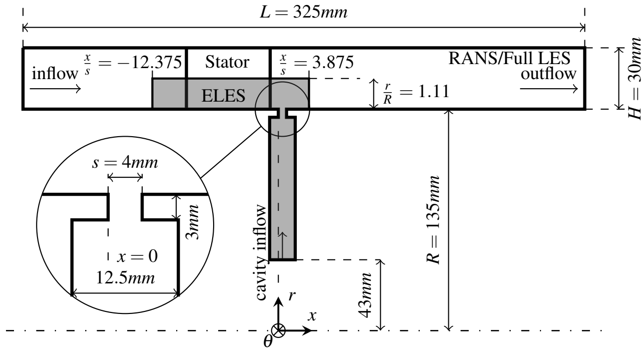

Figure 6. Schematic of the ICAS-GT2 stator cascade geometry with the first wheel space with the location of the embedded LES (ELES) region.

First, the turbine geometry and the computational setup are discussed. Then, a grid study is performed to find the grid resolution that accurately predicts the hot gas ingress and turbulent flow statistics relevant for hot gas ingress. Afterwards, the results for the embedded LES method adapted for curved turbine geometries are discussed and compared to the full LES and a preliminary RANS solution.

Geometry and numerical setup

The turbine consists of two stators with 16 vanes each and a rotor with 32 blades. Note that only the first stator row and the upstream wheel space are considered, whereas the rotor blades are not taken into account. The rotor is modeled inside the main annulus as a cylinder, inside the wheel space the rotor geometry is unchanged to obtain identical sealing lip geometries. Only one sector of the turbine geometry is considered using the azimuthal periodicity method by Hösgen *et al.* (2023). With 16 stator blades, the periodic azimuthal turbine angle is $\theta_\mathrm{P} = 22.5°$. To reduce the convergence time of the slow wheel space flow and in turn the computational cost of this investigation, the axial part of the wheel space at the lower rotor hub is neither considered.

Figure 6 shows a schematic of the investigated curved turbine cascade geometry superimposed with the embedded LES region, which encompasses the turbulent boundary layer upstream of the stator, the lower part of the stator blade, and the wheel space. The hub radius of the rotor is $R = 135$mm and the height of the main annulus is $H = 30$mm. The lower hub of the rotor is 43*mm*. The length of the main annulus is $L = 325$mm. The extent of the rim seal gap in the streamwise direction x is $s = 4$mm. The wheel space is symmetric with a double lip geometry. The inflow of the embedded LES region is located at $x/s = -12.375$. The position of the tangential zonal interface is set to $r/R = 1.11$ corresponding to half the channel height. The outflow of the embedded LES region is located at $x/s = 3.875$.

At the main annulus inflow, density and velocity are prescribed. In the full LES, synthetic turbulence with a turbulence intensity of 7% is imposed using the method of Batten *et al.* (2004). At the main annulus outlet, the pressure is fixed to p_out. At the wheel space cavity inlet, density and velocity are prescribed according to the specified sealing-air mass flux, without prescribed turbulence. At the stator and rotor surfaces, adiabatic no-slip conditions are applied, together with a Robin-type boundary condition for pressure and density.

The number of grid cells for the different simulation methods are summarized in table 2. The grid of the pure LES and pure RANS setup consists of 244 million cells. Here, the Spalart-Allmaras turbulence model is used. The zonal setup has a grid size of 76 million cells, corresponding to a reduction in grid cells of 69%.

Table 2. Number of grid cells employed for the different setups for the curved turbine cascade.

	RANS	LES	embedded LES
grid cells [10^6]	244	244	76

Simulation results

In the following, the cavity flow of the curved axial turbine is analyzed with special focus on the prediction of the cooling efficiency. Time- and spanwise-averaged radial distributions of key flow quantities within the wheel space are examined.

Figure 7 shows an instantaneous visualization of the Q-criterion, colored by velocity magnitude, within the embedded LES region, highlighting key turbulent features of the curved turbine cascade. The horseshoe vortex is visible around the stator leading edge, while the inflow boundary of the embedded LES domain is located just upstream of its formation. The turbulent stator wake is clearly resolved, with its structures extending up to the TZI boundary, indicating that the TZI does not impede the development of turbulence. Downstream of the stator cascade, interactions between secondary flow structures, i.e., the horseshoe vortex and the corner vortex, the turbulent stator wake, and the shear layer around the rim seal gap occur. The turbulent structures are able to leave the domain with minimal reflection through the NSCBC boundary condition.

The radial distributions of the time- and azimuthally averaged radial velocity component v_r, the pressure p, and the cooling effectiveness η are shown for two axial positions within the wheel space in figure 8. The cooling effectiveness η is defined as

$$\eta = \frac{Y(r) - Y_{\text{hg}}}{Y_{\text{cg}} - Y_{\text{hg}}}. \quad (6)$$

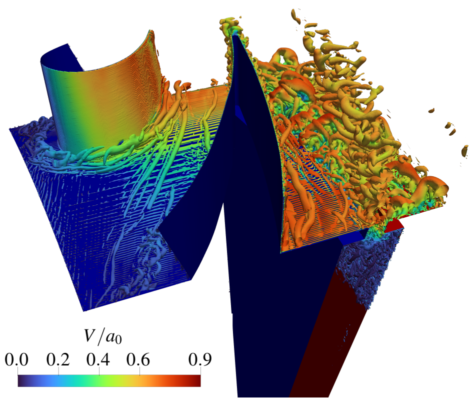

Figure 7. Q-criterion colored by the instantaneous velocity magnitude V of the embedded LES region. The stator wall is colored in blue, the rotor wall in red.

The quantity Y denotes the passive scalar concentration, with the passive scalar concentration in the hot gas $Y_{\text{hg}} = 0$ and the cooling gas concentration in the wheel space $Y_{\text{cg}} = 1$.The distributions at $x/s = -0.9375$, i.e., close to the stator wall, are presented in the left column. The right column shows the radial distributions near the rotor disk at $x/s = 1.9375$. It is shown that the cooling effectiveness is higher near the rotor wall than near the stator wall for the pure LES and embedded LES, with strong agreement between these methods. In combination with the radial velocity distributions, this indicates that the reduced hot gas ingress near the rotor wall is driven by increased radial outflow caused by rotor-induced acceleration in both azimuthal and radial directions. This outwash generates a recirculating vortex in the upper wheel space ($r/R > 0.9$), leading to negative time-averaged radial velocities near the stator wall causing an increase in hot gas ingress. The radial velocity is accurately captured by the embedded LES compared to the pure LES. The RANS solution also shows good agreement in radial velocity, with larger discrepancies primarily occurring in the lower wheel space. The RANS solution, however, predicts significantly reduced hot gas ingress near the stator wall and therefore a higher cooling effectiveness in this region. The combination of good agreement in the prediction of the radial velocity and significantly reduced hot gas ingress near the stator wall suggests deficiencies of the RANS model in predicting shear layer mixing. The pressure distributions from all three modeling approaches are in good agreement overall, with the pressure of the embedded LES closely matching the pressure obtained by the RANS solution due to the boundary formulation of the NSCBC. However, deviations between the embedded LES and RANS are observed within the cavity shear layer at $r/R \approx 1$, also indicating differences in predicted mixing behavior.

The shear layer dynamics and turbulent fluctuations of the cavity flow are analyzed using radial distributions of the Reynolds stress components relevant to hot gas ingress $\overline{v_r'v_r'}$ and the turbulent kinetic energy k, are also depicted in figure 8 at the two axial positions as discussed before. The embedded LES exhibits very strong agreement with the pure LES for all turbulent quantities with the exception of the differences in the main channel flow caused by the TZI formulation, where the radial velocity fluctuation is damped, i.e., $\overline{v_r'v_r'}|_{\text{TZI}} = 0$ and the subsequent shift of the turbulent fluctuations in the two interface-parallel directions.

CONCLUSION AND OUTLOOK

In this manuscript, an embedded LES method capable of resolving the highly complex multi-mode hot gas ingress into the stator-rotor cavity wheel space of axial turbine geometries has been presented. The method uses a preliminary pure RANS simulation of the flow case to provide meaningful boundary conditions for a reduced region of interest simulated by means of LES, e.g., in high-shear layer regions. The embedded LES is effectively used as a magnifying glass, providing locally high temporal and spatial resolution of specific flow features making it ideal to seamlessly integrate into the industrial design process of turbomachinery.

The embedded LES approach was first validated for the separating flow over a curved backward-facing step which features flow states similar to those expected in axial turbine applications. This includes an incoming turbulent boundary layer at the inflow, non-zero mass flux at the tangential boundary, and a highly turbulent flow with possible flow reversals at the outflow. The reduced LES domain has a cell reduction of 40%

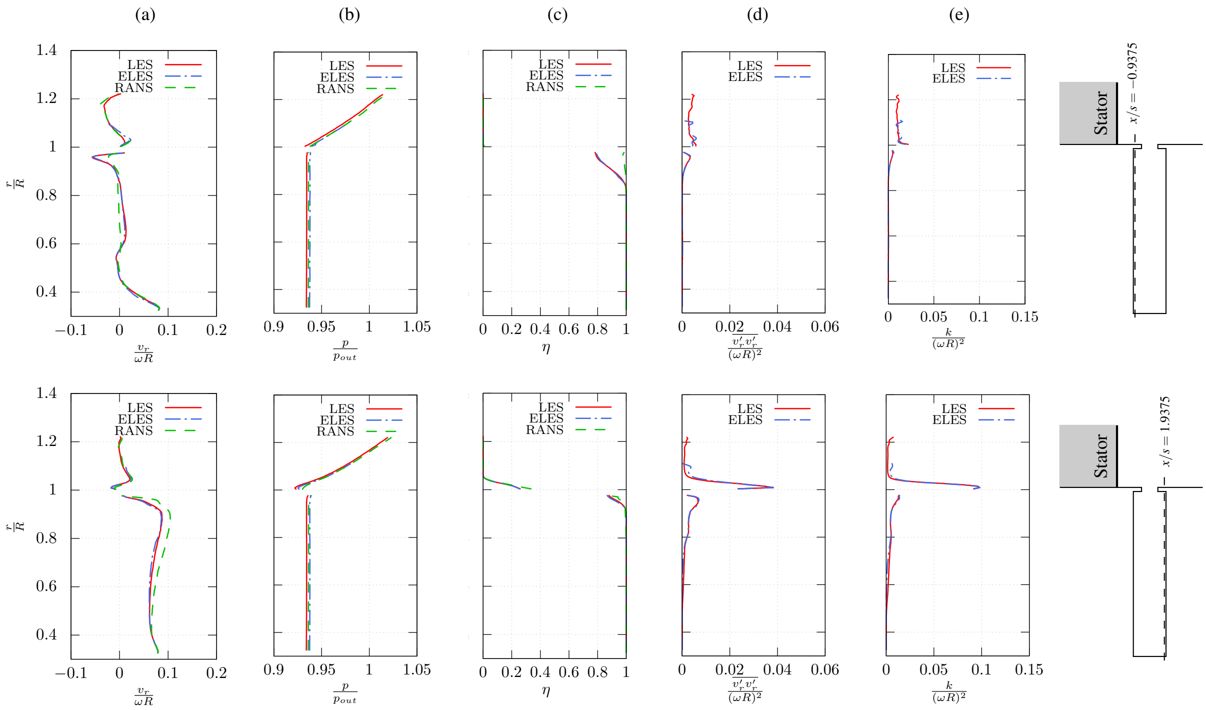

Figure 8. Time and azimuthal average for (a) the radial velocity component v_r, (b) the pressure p and (c) for the cooling effectiveness η, (d) the Reynolds stress component $\overline{v_r' v_r'}$, and (e) the turbulent kinetic energy k plotted over radial position r for (top) $x/s = -0.9375$, and (bottom) $x/s = 1.9375$. Fine: fine LES, RANS: pure RANS, ELES: embedded LES. A schematic of the axial positions is included on the right.

compared to the full LES domain. The separating flow was accurately captured by the embedded LES compared to the pure LES significantly improving upon the results obtained by RANS. The embedded LES method with the described changes for curved turbine geometries were subsequently validated for a curved turbine cascade, for which an overall reduction in grid cells of 69% compared to the pure LES were achieved. The cavity and main annulus flow were accurately predicted with a strong agreement in the hot gas ingress predictions compared to the pure LES setup.

REFERENCES

Batten, Paul, Chakravarthy, Sukumar & Goldberg, U. 2004 Interfacing Statistical Turbulence Closures with Large-Eddy Simulation. *AIAA Journal* **42**, 485–492.

Borgelt, Jannik, Meinke, Matthias & Schröder, Wolfgang 2025*a* Embedded les boundary conditions for shear dominated flows. *Computers & Fluids* **299**, 106729.

Borgelt, Jannik, Meinke, Matthias, Schröder, Wolfgang & Krug, Dominik 2025*b* An embedded zonal les method applied for predictions in turbomachinery applications. In *Proceedings of the 15th ERCOFTAC Symposium on Engineering Turbulence Modelling and Measurements (ETMM15)*, pp. 380–385. ERCOFTAC.

Gao, Feng, Chew, John W., Beard, Paul F., Amirante, Dario & Hills, Nicholas J. 2018 Large-eddy simulation of unsteady turbine rim sealing flows. *International Journal of Heat and Fluid Flow* **70**, 160–170.

Granet, Victor, Vermorel, Olivier, Léonard, Thomas, Gicquel, Laurent & Poinsot, Thierry 2010 Comparison of Nonreflecting Outlet Boundary Conditions for Compressible Solvers on Unstructured Grids. *AIAA Journal* **48** (10), 2348–2364.

Hösgen, Thomas, Meinke, Matthias & Schröder, Wolfgang 2023 Analysis of single-blade passage and full circumference large-eddy simulations of turbine rim seal flows. *Journal of Turbomachinery* **146** (4), 041002.

Hösgen, Thomas, Meinke, Matthias & Schröder, Wolfgang 2024 Analysis of ingress into the downstream wheel space of a 1.5-stage turbine by full circumference and single blade passage large-eddy simulations. *Journal of Turbomachinery* **146** (9), 091006.

Jakoby, Ralf, Zierer, Thomas, Lindblad, Klas, Larsson, Jonas, deVito, Laurent, Bohn, Dieter E., Funcke, Joachim & Decker, Achim 2004 Numerical simulation of the unsteady flow field in an axial gas turbine rim seal configuration **4**, 431–440.

Langley Research Center 2021 Turbulence Modeling Resource. Accessed: 2025-01-03.

O'Mahoney, T S D, Hills, N J, Chew, J W & Scanlon, T 2011 Large-eddy simulation of rim seal ingestion. *Proceedings of the Institution of Mechanical Engineers, Part C: Journal of Mechanical Engineering Science* **225** (12), 2881–2891.

Pogorelov, Alexej, Meinke, Matthias & Schröder, Wolfgang 2019 Large-eddy simulation of the unsteady full 3d rim seal flow in a one-stage axial-flow turbine. *Flow, Turbulence and Combustion* **102**.

Rabs, M., Benra, F.-K., Dohmen, H. J. & Schneider, O. 2009 Investigation of flow instabilities near the rim cavity of a 1.5 stage gas turbine. *Turbo Expo*, vol. Volume 3: Heat Transfer, Parts A and B, pp. 1263–1272.

Roidl, B., Meinke, M. & Schröder, W. 2013 A reformulated synthetic turbulence generation method for a zonal RANS–LES method and its application to zero-pressure gradient boundary layers. *International Journal of Heat and Fluid Flow* **44**, 28–40.